Molecular Therapy
Nucleic Acids
Original Article

The beauty of symmetry: siRNA phosphorodithioate modifications reduce stereocomplexity, ease analysis, and can improve *in vivo* potency

Sophie Schöllkopf,[1,2] Stefan Rathjen,[1,2] Micaela Graglia,[1] Nina Was,[1] Eliot Morrison,[1] Adrien Weingärtner,[1] Lucas Bethge,[1] Judith Hauptmann,[1] and Marie Wikström Lindholm[1]

[1]Silence Therapeutics GmbH, Robert-Rössle-Street 10, 13125 Berlin, Germany

Phosphorothioates (PSs) can be essential in stabilizing therapeutic oligonucleotides against enzymatic degradation. However, unless synthesis is performed with stereodefined amidites, each PS introduces a chemically undefined stereocenter, resulting in 2^n unique molecules in the final product and affecting downstream analytics and purification. Replacing the second non-bridging oxygen with sulfur results in phosphorodithioate (PS2) linkages, thereby removing the stereocenter. We describe synthesis and analytical data for *N*-acetylgalactosamine (GalNAc)-conjugated small interfering RNAs (siRNAs) with PS2 in the GalNAc cluster and at the siRNA termini. All siRNA conjugates with PS2 internucleotide linkages were produced with good yield and showed improved analytical properties. PS2 in the GalNAc cluster had no, or only minor, effect on *in vitro* and *in vivo* activity. Except for the 5′-antisense position, PS2 modifications were well tolerated at the siRNA termini, and a single PS2 internucleotide linkage gave similar or improved stabilization and *in vitro* activity as the two PSs typically used for end stabilization. Surprisingly, several of the PS2-containing siRNA conjugates resulted in increased *in vivo* activity and duration of action compared to the same siRNA sequence stabilized with PS linkages, suggesting PS2 linkages as interesting options for siRNA strand design with a reduced number of undefined stereocenters.

INTRODUCTION

Therapeutic small interfering RNAs (siRNAs) are frequently stabilized against *in vivo* degradation to exert the intended effect. This is essential for siRNA conjugation to, for instance, *N*-acetylgalactosamine (GalNAc), which requires position-dependent siRNA strand stabilization to resist nuclease-mediated degradation during delivery to its cytosolic mRNA target site. siRNAs are frequently stabilized with phosphorothioate (PS) internucleotide linkages. The exchange of one non-bridging oxygen in the phosphodiester bond breaks the symmetry of the linkage between the nucleotides.[1] Independent of the chosen stabilization chemistry, an additional stereocenter is created. If the absolute configuration of the P(III)-triester species during coupling is not controlled before it is oxidized to the P(V)-triester, both isomers with the resulting S_p and R_p configuration will be formed,[2,3] resulting in a complex isomeric mixture of the oligonucleotide product. siRNAs with stereodefined PSs can exhibit different levels of efficacy *in vitro* and *in vivo* in a position-specific manner.[2–4] For example, R_p isomers are more prone to enzymatic degradation than S_p isomers,[5] and R_p isomers at the 5′-antisense termini are preferred for improved interactions with Ago2.[2–4] Such stereoisomer species also feature varied physicochemical properties, resulting in complex and broadened chromatographic peak structures that in turn can negatively impact purification efficacy and downstream analysis of the product. If control methods to analyze the detailed diastereomer distribution are lacking, it is possible that batch-to-batch variability in the content of certain stereoisomer species in the oligonucleotide product could go unnoticed.[6] Although the use of PSs with uncontrolled stereochemistry for PS linkages has already led to the development of safe and effective medicines approved for indications with prior unmet medical need,[7] individual siRNA strands could further benefit from optimized oligonucleotide synthesis with a controlled absolute configuration for the reasons outlined above. Using chiral amidites, it is possible to synthesize each PS internucleotide linkage in an R_P or S_P configuration, and several approaches to this end have been published recently.[8–10] However, this may require a large set of compounds to be synthesized and screened to establish optimal conformation for each sequence. An alternative approach to introduction of stereodefined PS internucleotide couplings is to replace the second non-bridging oxygen with a sulfur, which results in a phosphorodithioate (PS2) internucleotide linkage. This approach, in part with the rationale of removing undefined stereocenters, was already described in 1989 by Caruthers et al.,[11] suggesting that PS2 can be an attractive analog to phosphodiester. PS2 has since been reported to provide strong metabolic stability and functional tolerance in siRNAs, although mainly in the context of unmodified siRNAs and with no clear positional dependence.[12–15] Additionally, only relatively small, low-complexity screens are required to explore the full property space. We sought to explore the use of PS2

Received 18 June 2024; accepted 5 September 2024;
https://doi.org/10.1016/j.omtn.2024.102336.

[2]These authors contributed equally

Correspondence: Marie Wikström Lindholm, Silence Therapeutics GmbH, Robert-Rössle-Str. 10, 13125 Berlin, Germany.
E-mail: m.lindholm@silence-therapeutics.com

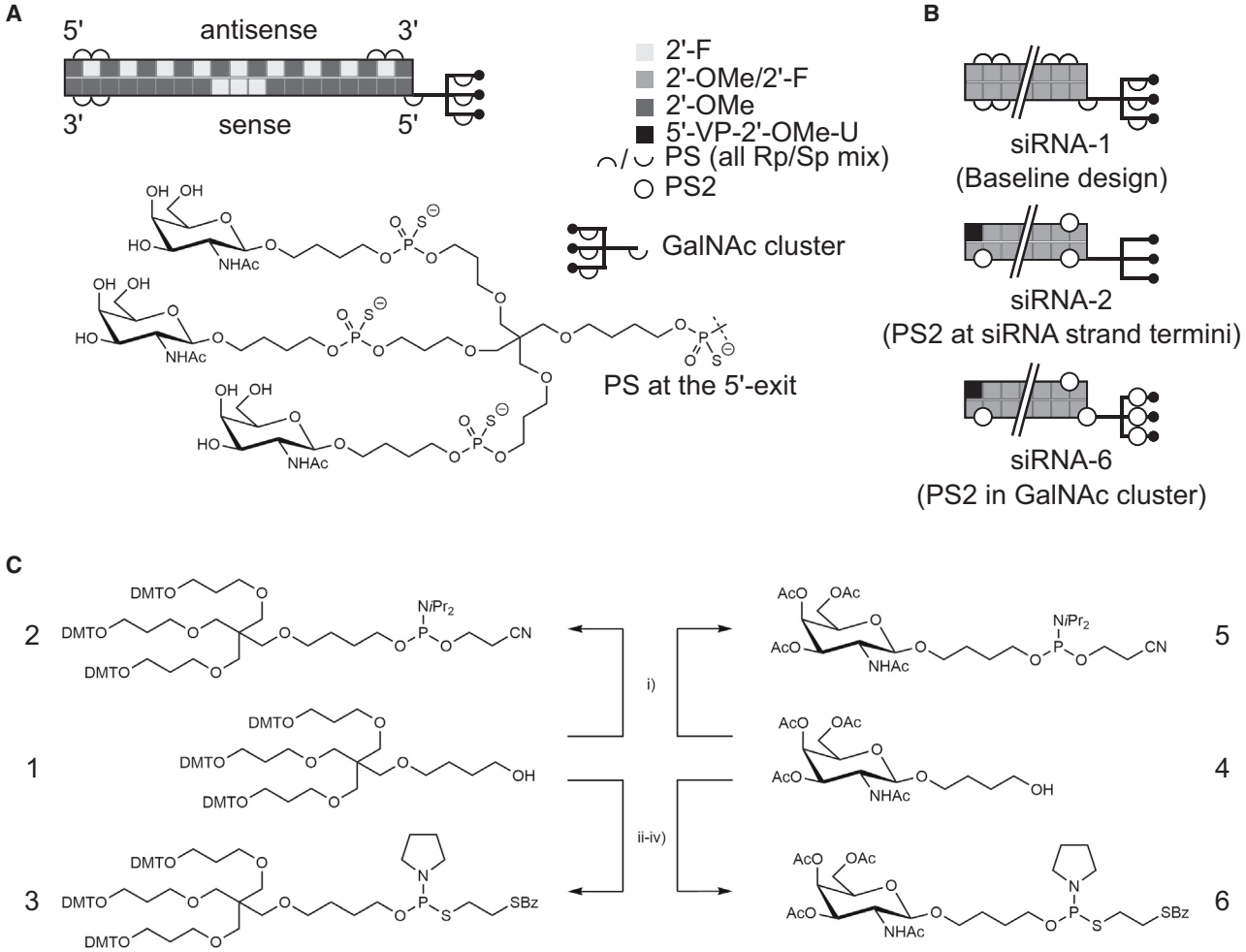

Figure 1. Baseline design, end-stabilization pattern, and building-block synthesis

(A) Baseline design of a GalNAc-conjugated siRNA and chemical structure of the GalNAc cluster that have been used to introduce phosphorodithioate modifications. (B) Examples of condensed cartoons representing siRNA conjugate design with PS and PS2 linkages for end stabilization (siRNA-2) and GalNAc-cluster modification (siRNA-6). All condensed cartoons specify where the siRNAs differ from the baseline design. (C) Reaction schemes for building blocks for the GalNAc clusters modified with phosphorodithioate.

internucleotide linkages to reduce the number of stereoisomer species in the final oligonucleotide product. Here, we give examples of synthesis, analytics, stability, and pharmacokinetic-pharmacodynamic (PK-PD) properties for variants of a GalNAc-siRNA targeting antithrombin III (AT3)[16] replacing PS with PS2 at different terminal positions of the siRNA strands, and in some cases also replacing PS by phosphodiester (PO). In contrast to others,[17] we are using a solid-phase phosphoramidite synthesis approach to build the triantennary GalNAc cluster, which leads to the opportunity to use PS linkages for further stabilization. Due to the branching nature of the GalNAc cluster, up to four thiolations can be introduced in the cluster alone; to explore the effect of reducing and/or replacing PS linkages in the cluster, several dithiolated cluster candidates were synthesized. The properties of these molecules, including siRNA analytics, siRNA stability, *in vitro* activity, and *in vivo* performance, were assessed and compared to a baseline design featuring a total of ten undefined PS stereocenters (Figures 1A and 1B). Overall, introducing PS2 to reduce the number of undefined stereocenters in either the sequence termini or the GalNAc cluster had a position-dependent effect on synthesis, analytics, metabolic stability, and *in vitro* as well as *in vivo* activity. The effect was most pronounced when PS2 was introduced at the siRNA strand termini, with only minor effects in the GalNAc cluster. Notably, the new designs include examples wherein siRNA end stabilization by two PS internucleotide linkages can be replaced by one single PS2 with retained or improved molecular properties. These results indicate that the introduction of PS2 in selected positions of GalNAc-conjugated siRNAs provides a viable option to minimize undefined stereocenters and simplify the stereoisomer mixture of the oligonucleotide product while maintaining, or even enhancing, functional properties of the molecule.

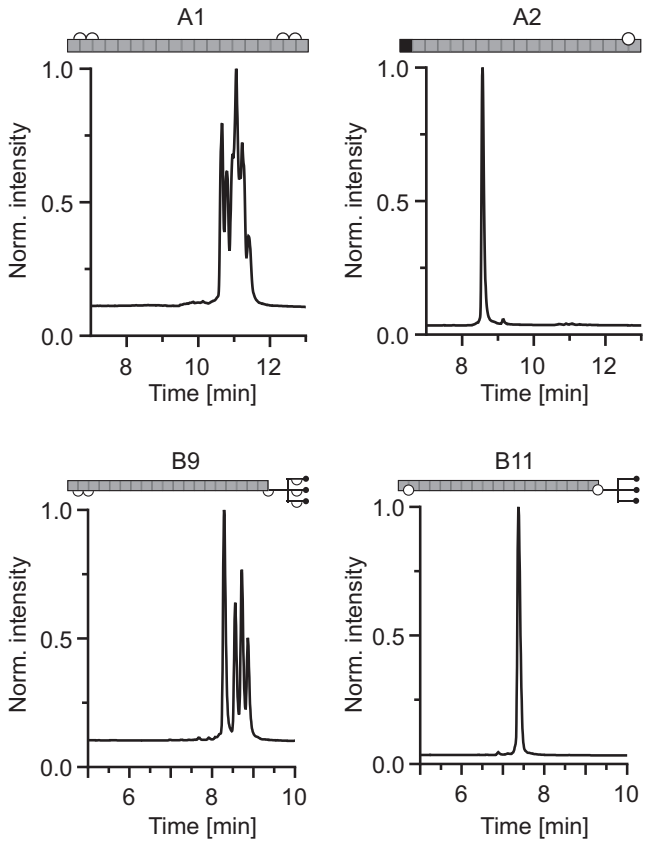

Figure 2. PS2 modifications reduce stereocomplexity and simplify analysis of GalNAc-siRNA conjugates

Chromatograms obtained by AEX analytical method e (Table S1) showing the different peak shapes of PS-modified (stereomixed) and PS2-modified (stereopure) antisense (A1, A2) and GalNAc-conjugated sense (B9, B11) strands.

RESULTS

Synthesis of PS2-modified GalNAc clusters and oligonucleotides

The synthesis of PS2-modified oligonucleotides was achieved using thiophosphoramidites with a standard phosphoramidite-based oligonucleotide solid-phase synthesis cycle with slight alterations. While 2′-OMe- and 2′-F-modified RNA-phosphoramidites and thiophosphoramidites are commercially available, additional synthesis of the branching and GalNAc building blocks was required. Synthesis of the trebler-phosphoramidite (**2**, Figure 1C) and GalNAc-phosphoramidite (**5**, Figure 1C) was achieved in good yield and purity as described elsewhere.[18] Literature-reported synthesis routes for nucleoside thiophosphoramidites[19] could be adopted for the generation of the trebler-phosphoramidite (**3**, Figure 1C) and GalNAc thiophosphoramidite (**6**, Figure 1C). Both thiophosphoramidites **3** and **6** showed relatively poor chemical stability at ambient conditions. Therefore, during oligonucleotide synthesis, both amidite solutions were freshly prepared prior to their use in the coupling step. Using the aforementioned protocol, synthesis of PS2-containing GalNAc clusters was executed successfully, albeit with reduced coupling efficiency and crude yield.

The reported lower coupling efficacy of thiophosphoramidites made it necessary to optimize the coupling cycle for their addition. In contrast to literature reports,[20] we found 0.3 M 5-benzylthiotetratzole (BTT) to be the most effective activator in the coupling of thiophosphoramidites. Coupling efficacy was additionally improved when a double equivalent supply over standard nucleoside phosphoramidites split in a triple couple-wash cycle of 3 × 20 min was used. The coupling of 2′-OMe-rG(ibu) remained poor even under these conditions.

PS2 linkages improved peak shapes in oligonucleotide analytics

The distribution of different isomers in an oligonucleotide with PS linkages can be revealed by chromatographic anion exchange chromatography (AEX) methods. Here, a DNA Pac PA200RS column was used, as it can separate and distinguish oligonucleotide diastereomers (method e, Table S1).[21] The antisense strand of our baseline design with two PS in each terminus and, hence, 2^4 isomers, was compared to an antisense strand with a single PS2 at each terminus (Figure 2, strands A1 and A2). The baseline design resulted in a broad (over 1 min) and complex peak shape. Replacing PS with PS2 and PO results in a narrow and sharp peak shape. The same result can be achieved with the sense strand. Here, in the sense strand B9 PS modifications are placed on the 3′ end in the strand (2× PS) as well as in the GalNAc cluster (4× PS). This way, the peak shape is heavily broadened and shows a quaternary peak (Figure 2, strand B9). Once all undefined stereocenters are replaced by either PO or PS2 linkages, the peak shape is improved to a single peak (Figure 2, strand B11). As both PS and PS2 modifications have been described to affect thermal properties of siRNAs,[22,23] the PS2-modified siRNA conjugates were subjected to thermal stability measurements (Figure S1). All duplexes showed a sigmoidal curve when absorption was measured at 260 nm with a temperature ramp (Figure S1). Interestingly, measured and calculated T_m values differ around ±1 K per siRNA. In general, it could be shown that replacing two PSs by one PS2 at the strand termini barely affected thermal stability of the duplex.

PS2 modification of the GalNAc cluster affects conjugate stability in a position-dependent manner

The "baseline design" introduced here is a blunt-ended 19-mer siRNA with all riboses modified with 2′-OMe or 2′-F, with two PS internucleotide linkages stabilizing the 5′ antisense, 3′ antisense, and 3′ sense strands, respectively, and with four PS linkages in the GalNAc cluster (siRNA-1, Figures 1A and 1B). All investigated variations of the baseline design were blunt-ended 19-mers with the same ribose-modification pattern, i.e., based on siRNA-1. To investigate the impact of PS2 in the GalNAc cluster, PSs were replaced by PO, after which PS2 modifications were introduced to the GalNAc cluster in a stepwise manner. To eliminate the impact of PS groups in sense and antisense strands, we designed a set of molecules that had no undefined stereogenic centers in the siRNA strands (siRNA-2 to siRNA-8, Figure 3A), allowing for us to test whether PS2 is tolerated

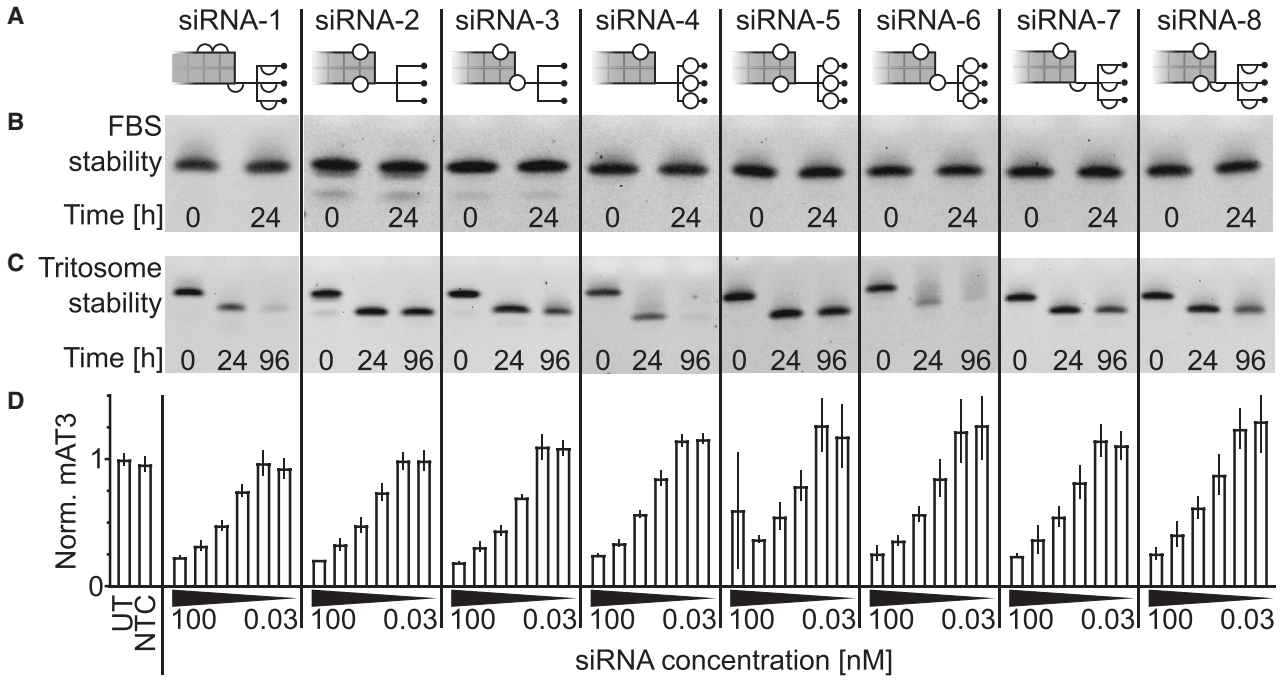

Figure 3. *In vitro* serum and tritosome stability and *in vitro* efficacy of PS2 GalNAc-cluster variants

(A) Cartoon representations of GalNAc-cluster variants. Half circles depict PS and full circles PS2. PAGE analysis after (B) serum and (C) tritosome stability assays run for 0, 24, and 96 h. (D) Knockdown efficacy in mouse primary hepatocytes after 24 h. AT3 expression was normalized to ApoB and actin. Data represent the geometric mean (SD) of three technical replicates. UT, untreated sample; NTC, non-targeting control.

or possibly beneficial in an internucleotide position at the 5′ end of the passenger strand, or between the final 5′ passenger strand ribose position and the GalNAc cluster, or within the GalNAc cluster.

To predict the stability in circulation, GalNAc-siRNA conjugates were incubated for 0 or 24 h in fetal bovine serum (FBS) at 37°C. Subsequently, electromobility was compared in PAGE analysis. For all tested conjugates, band intensities between the 0- and 24-h time points did not change substantially, suggesting that the conjugates are stable in serum for the time frame relevant for circulation and uptake (Figure 3B).[24]

After endocytosis, GalNAc-siRNA conjugates are assumed to dissociate from the receptor and are intracellularly processed for degradation via the endolysosomal pathway.[25,26] To mimic the endo-lysosomal milieu, we challenged the stability of siRNA conjugates by incubation in acidified rat liver tritosome lysates for up to 4 days at 37°C with subsequent PAGE analysis (Figure 3C). In contrast to serum, all tested conjugates showed a characteristic band shift when incubated in rat liver tritosomes comparing 0 and 24 h time points. As reported earlier, this can be explained by glycosidic bond cleavage of GalNAc sugars from the linker (Figure S2).[26,27] After 96 h in rat liver tritosomes, most siRNA conjugates did not show further band shifts, suggesting longer-term stability of the siRNA duplex in the endolysosomal pathway (Figure 3C). Baseline design siRNA-1 revealed a decreased band intensity after 96 h, and siRNA-6 showed a quicker decay already starting after 24 h. Among the tested conjugates, siRNA-4 was the only conjugate with a different band shift, suggesting a different stable metabolite. In high-performance liquid chromatography (HPLC) coupled with mass spectrometry (MS), we were able to identify masses that correlate with the loss of the GalNAc cluster and up to two nucleotides at the 5′ end of the sense strand (Figure S2A). siRNA-4 is strongly degraded after 96 h of tritosome incubation, suggesting that either the 5′ end or the 5′ exit of the sense strand require stabilization by PS2.

To analyze the impact of PS2-containing GalNAc variants on activity of GalNAc-conjugated siRNA, we addressed knockdown efficacy in primary hepatocytes via receptor-mediated uptake. After 24 h of incubation with the indicated siRNA conjugates at concentrations ranging from 0.03 to 100 nM, mRNA levels of AT3 were measured by qPCR. Overall, all conjugates showed a concentration-dependent knockdown of AT3, decreasing the target mRNA level by about 50% at 4 nM siRNA concentration. All PS2-containing GalNAc-cluster variants were well tolerated, with no effect on the *in vitro* knockdown efficacy (Figure 3D).

5′-Sense strand stabilization is required for *in vivo* activity for PS2 in GalNAc cluster

With all GalNAc-cluster variants showing similar *in vitro* efficacy, *in vivo* activity for the different variants was tested in wild-type mice. C57BL/6 male mice were administered subcutaneously

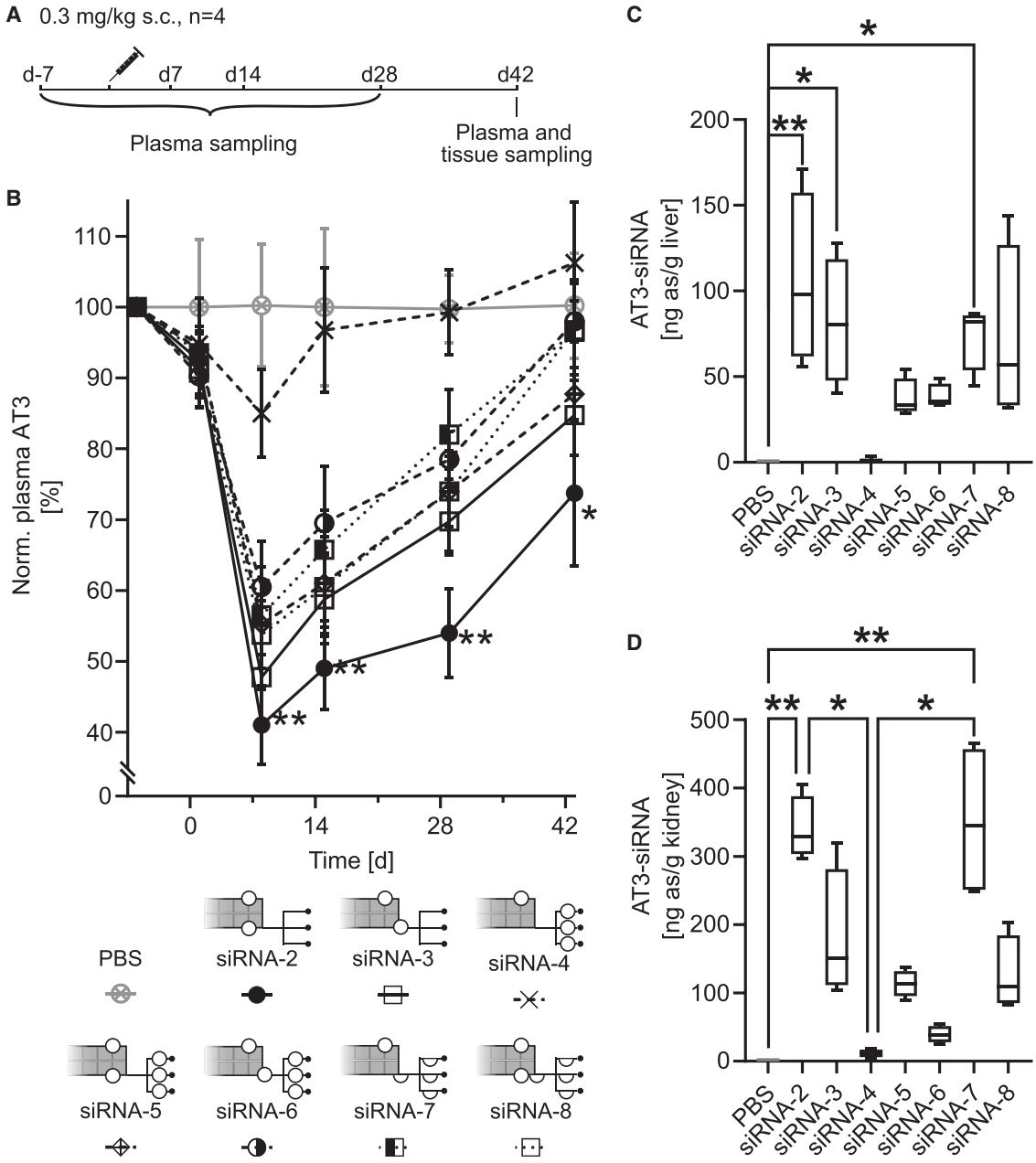

Figure 4. *In vivo* siRNA efficacy in liver and siRNA content analysis in liver and kidney

(A) *In vivo* study design. Male C57BL/6 mice (n = 4/group) were injected subcutaneously with 0.3 mg/kg GalNAc-siRNA conjugates. Plasma AT3 and liver and kidney siRNA levels were analyzed as indicated. (B) Plasma AT3 levels were normalized to individual pre-dose as well as to the mean of PBS-treated animals at the respective time point. Data represent the mean (SD). One-way ANOVA statistical analysis was performed comparing the mean rank of siRNA-2 against PBS by Kruskal-Wallis test with Dunn's multiple comparison at respective time points. Asterisks indicate number of digits after the decimals for p values. The levels of the siRNA antisense strand in (C) liver and (D) kidney lysates were determined by stem-loop RT-qPCR 6 weeks after treatment. Shown are medians in box and whiskers. One-way ANOVA statistical analysis was performed by comparing the mean rank of each treatment cohort against every other by Kruskal-Wallis test with Dunn's multiple comparison at respective time points. Asterisks indicate digits after the decimals for p values.

0.3 mg/kg GalNAc-siRNAs targeting AT3 (Figure 4A). EDTA-plasma levels of AT3 were measured over the time course of 6 weeks (Figure 4B). AT3 plasma levels correlate well with AT3 mRNA levels in liver, thus providing a biomarker of effect.[16] The PBS group and plasma samples from 7 days before injection were used for normalization. Overall, the nadir of AT3 plasma protein level was reached

1 week after injection. Two to four weeks after treatment, only siRNA-2 and siRNA-3 demonstrated significant downregulation of AT3 plasma levels when normalized to respective pre-dose level and to PBS control levels at each time point (Figure 4B). Following week 1, AT3 plasma levels started to return to baseline. This finding confirms the importance of 5′-strand end or 5′-exit stabilization, as indicated by the tritosome stability analysis (Figure 3C). At the final time point, only siRNA-2 demonstrated significant knockdown, ending the study at 74% ± 10.3% AT3 levels, suggesting a longer duration of action (Figure 4B). We next asked whether siRNA activity correlated with the amount of siRNA present in tissue. For this, the level of siRNA antisense strand in liver lysates was quantified in tissue samples from day 43 by stem-loop RT-qPCR (Figures 4C and 4D). At this time point only cohorts treated with siRNA-2 (105.7 ± 50.1 ng siRNA/g liver), siRNA-3 (82.3 ± 36.8 ng siRNA/g liver), and siRNA-7 (73.7 ± 19.5 ng siRNA/g liver) were significantly different from the PBS group (Figure 4C). Although plasma AT3 protein reduction correlated well for siRNA-2 with remaining siRNA in total liver lysate, this was not the case for siRNA-3 and siRNA-7.

The amount of siRNA in the kidney 6 weeks after injection was also quantified (Figure 4D). Overall, the siRNA content was two to three times higher in kidney than in liver. As the target gene, AT3, is not expressed in kidney, functional knockdown could not be assessed in this tissue. However, previous studies with a ubiquitously expressed target did not show functional knockdown in kidney (data not shown). siRNA-7 with a PS-stabilized GalNAc cluster and siRNA-2, the highly potent, stereopure conjugate featuring a PO cluster, showed the highest levels of kidney accumulation at 350.9 ± 113.7 ng siRNA/g and 340.0 ± 46.6 ng siRNA/g kidney, respectively. Overall, kidney accumulation does not seem to be determined by the GalNAc-cluster thiolation or the lack thereof.

Taking everything together, GalNAc clusters where GalNAc building blocks were linked by non-stereogenic POs and PS2 modification were placed at the 5′-sense strand end or the 5′-sense strand exit that links to the trebler (siRNA-2 and siRNA-3) performed best compared to PS-linked stereomixed GalNAc clusters (siRNA-7 and siRNA-8) or PS2-modified GalNAc clusters (siRNA-4, siRNA-5, and siRNA-6). However, it must be stated that PS2 modifications are as well tolerated as PS modifications in the GalNAc cluster as long as sufficient overall metabolic stability of the conjugate is achieved. The non-thiolated cluster with 5′-sense strand end stabilization (siRNA-2) outperformed the thiolated clusters in initial knockdown efficacy, duration of action, and enhanced liver accumulation.

In vitro analysis of GalNAc-siRNA conjugates with siRNA strand PS2 modifications

Next, it was explored whether PS2 linkages could functionally substitute for PS linkages used for stabilization of the siRNA termini, thereby possibly improving stability and/or activity due to reduced stereoisomeric complexity. All investigated variations of the baseline design (Figure 1A) were blunt-ended 19-mers with the same ribose-modification pattern, i.e., based on siRNA-1. GalNAc-siRNA conjugates with 2× PS, 1× PS, and 1× PS2 at each of the non-conjugated ends were tested in stability assays with rat liver tritosomes (Figure 5A). Interestingly, tritosome stability of siRNA conjugates with single terminal PS2 linkages was comparable to that of conjugates with two terminal PS linkages (siRNA-1 and siRNA-9), whereas an siRNA conjugate with one terminal, PS showed reduced stability (siRNA-10). Stability of the siRNA conjugate was additionally improved when an additional PS2 was used at the linker-conjugated terminus (siRNA-11). The GalNAc cluster of this conjugate did not contain any PS stabilizations (siRNA-2, Figure 3A). Next, the compatibility of PS2 modifications at the individual siRNA termini with RNAi function was investigated. To this end, GalNAc-siRNA conjugates with 2× PS at the individual termini were tested while all other termini were modified with 1× PS2 (Figure 5B). Knockdown activity of these siRNA conjugates was tested in mouse primary hepatocytes by receptor-mediated uptake, and target mRNA reduction was strongest when there was no PS2 at the 5′ antisense (siRNA-12). All other variants had comparable activity (Figure 5B). Taken together, these experiments suggest that 1× PS2 can substitute for 2× PS at the siRNA termini, and that PS2 is not well tolerated at the 5′ end of the antisense strand.

As the stereopure PS2 end stabilization was well tolerated at all siRNA termini but that of the 5′-antisense strand, an alternative way to remove the remaining stereogenic center at the 5′ end of the antisense strand was considered. One preferred modification at this site is 5′-E-vinylphosphonate (VP), which has been reported to confer both stability and, as a stable mimic of 5′-antisense phosphorylation, increased binding affinity to the MID domain of Ago2.[28–30] We have previously observed that with our baseline modification patterns the greatest improvement, when including VP in the 5′ antisense position, to on-target activity was achieved when PS internucleotide linkages at the neighboring nucleotides were replaced with PO linkages.[31] Tritosome stability of the siRNA duplex was enhanced when PS2 and VP were combined, with no PS or PS2 needed for additional stabilization of the 5′ antisense (Figure 5C). The stability of siRNA-1 was used as a baseline for all comparisons. Modification with VP at the 5′ antisense increased tritosome stability (siRNA-16, Figure 5C). Likewise, tritosome stability of the siRNA conjugate with PS2 modifications at all tolerated ends was further increased when combined with VP at the 5′ antisense (compare siRNA-17 to siRNA-12, Figure 5C). We tested RNAi activity of these conjugates after receptor-mediated uptake in mouse primary hepatocytes (Figure 5D). The 5′-VP modification improved knockdown activity of both the PS-modified and the PS2-modified conjugates (Figure 5D). Importantly, siRNA-17 reduced target gene levels at least as much as siRNA-16 (Figure 5D). Taken together, a GalNAc-siRNA conjugate without undefined stereogenic centers and with enhanced stability and improved on-target activity *in vitro* was identified.

In vivo analysis of GalNAc-siRNA conjugates with siRNA strand PS2 modifications

To test whether the enhanced stability and knockdown activity for PS2- and VP-modified siRNA conjugates observed *in vitro*

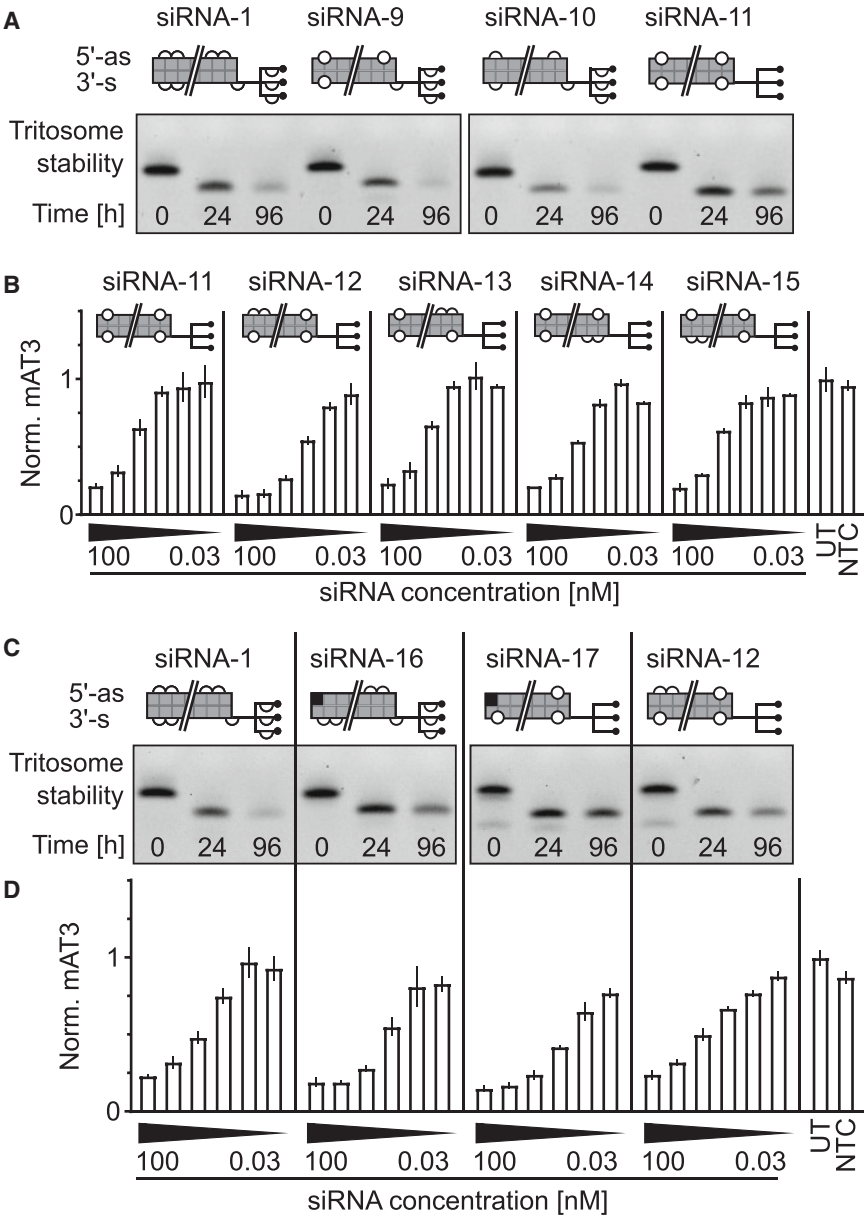

Figure 5. Single PS2 internucleotide linkages stabilize siRNA conjugates at their termini and increase activity *in vitro*

(A) Tritosome stability of siRNA conjugates with 2 PS, 1 PS, or 1 PS2 at the indicated siRNA termini. PS2-stabilized siRNA conjugates were tested with a PS-containing GalNAc cluster and with a PO-containing GalNAc cluster. Data for siRNA-1 are identical in (A), (C), and Figure 3C; all tritosome stability analyses used for these figures were run in the same experiment with the same siRNA-1 data as baseline control. (B) Functional tolerance for PS2 at the individual termini was analyzed by receptor-mediated uptake of the siRNA conjugates in mouse primary hepatocytes and analysis of target gene repression. AT3 expression was normalized to ApoB and actin. Data represent the geometric mean (SD) of three technical replicates. (C) Tritosome stability of siRNA conjugates with combinations of VP, PS2, and PO-containing GalNAc moiety as indicated. (D) The *in vitro* activity of siRNA conjugates with the indicated combinations of VP, PS2, and PO-containing GalNAc moiety was analyzed by receptor-mediated uptake in mouse primary hepatocytes. AT3 expression was normalized to ApoB and actin. Data represent the geometric mean (SD) of three technical replicates. UT, untreated sample; NTC, non-targeting control.

translates to an *in vivo* context, c57BL/6 mice were treated subcutaneously with 1 mg/kg of the previously described GalNAc-siRNA conjugates (Figure 6A). Target knockdown was followed by quantification of AT3 protein in EDTA-plasma over 49 days (Figure 6B). The PS-stabilized siRNA conjugate (siRNA-1) showed the least knockdown activity. Substitution of 5′-antisense PS by VP (siRNA-16) or replacing all 3′-PSs and the 5′-sense PS by single PS2 linkages, and replacing PS in the GalNAc-linker by PO (siRNA-12), resulted in approximately the same improvement in knockdown. AT3 knockdown was most pronounced for the combination of VP at the 5′ end of the antisense with PS2 at all other termini and the PO GalNAc-cluster (siRNA-17), possibly due to an additive improvement by combining VP and PS2. For this dose the maximum detected knockdown was reached 7 days after treatment. Overall, PS2-stabilized siRNA conjugates showed a stronger initial knockdown and a longer duration of action compared to PS-stabilized siRNA conjugates (Figure 6B).

To investigate this further, we quantified antisense strands in plasma, liver, and kidney by size-coded ligation-mediated PCR in tissue lysates at various time points following subcutaneous administration. Exploratory plasma sampling at 30 min to 4 h ($n = 2$) after injection suggested a similar clearance rate for all tested compounds, with a maximal plasma concentration at the earliest tested time point (data not shown). Although siRNA was detectable in plasma up to day 21 post treatment, the concentration at 4 h after treatment was almost 100-fold lower than at c_{max} (data not shown). In liver and kidney, initial levels of 4–10 μg siRNA/g tissue were reached after 24 h (Figures 6C and 6D). At later time points, PS2-stabilized siRNA-12 and siRNA-17 remained at higher concentrations in liver and kidney than PS-stabilized siRNA-1 and siRNA-16 (Figures 6C and 6D). The effect was even more pronounced in kidney, where 6 weeks after administration about 5 μg of siRNA/g kidney was still detectable. Following day 7, elevated siRNA levels of VP- and PS2-modified siRNA-17 in liver correlated well with improved reduction in circulating AT3 protein (Figures 6B and 6C).

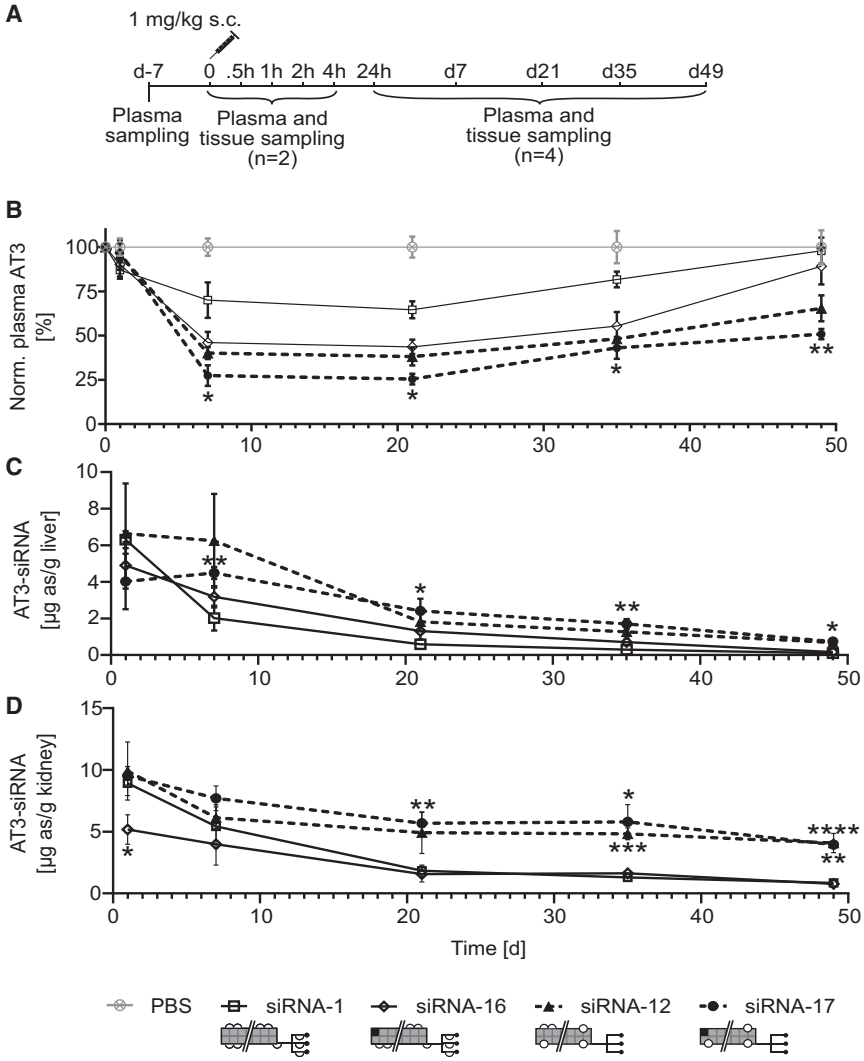

Figure 6. PK-PD of PS2 siRNA conjugates in liver and kidney

(A) Study design: male C57BL/6 mice were injected subcutaneously with 1 mg/kg GalNAc-conjugated siRNA. n = 4/group for all data except for explorative PK analysis during the first 4 h after injection (n = 2). (B) Plasma AT3 levels were normalized to individual pre-dose level as well as to the mean of PBS-treated animals at the respective time points. Data represent the mean (SD). One-way ANOVA was performed by comparing the mean rank of each treatment cohort against that of siRNA-1 by Kruskal-Wallis test with Dunn's multiple comparison at respective time points. Asterisks indicate the number of digits after the decimals for p values. AT3 antisense strands were quantified in liver (C) and kidney (D). Data represent the mean (SD). One-way ANOVA was performed comparing the mean values of each treatment group with the mean of siRNA-1 cohort at the respective time point by Brown-Forsythe ANOVA test and Welch's ANOVA test with Dunnett's T3 multiple comparisons test. Asterisks indicate the number of digits after the decimals for p values.

DISCUSSION

Here, we aimed to reduce the number of undefined stereocenters in a GalNAc-conjugated siRNA (Figure 1A) by substituting stereochemically undefined PS linkages for symmetric non-stereogenic PS2 or PO linkages. Synthesis of such PS2-modified oligonucleotides was previously reported only at very small scales (0.2–1.3 µmol) and required the use of a high excess of respective building blocks (40×) to yield reliable results.[20] In this work, we demonstrate a way to improve the introduction of PS2 in the siRNA strands and the GalNAc cluster during solid-phase synthesis. We synthesized and tested GalNAc-siRNA conjugates with PS2 at different positions of the GalNAc cluster. *In vitro* activity of these conjugates was comparable to that of molecules with PO or PS linkages (Figure 3). In addition, we tested the stability of GalNAc cluster variants in serum and rat liver tritosomes to simulate their behavior in blood and the endolysosomal pathway, respectively. While all tested compounds were stable in serum, the rapid loss of GalNAc sugars in tritosome extracts was not prevented by the introduction of PS2 at any site. In the tested siRNA conjugate lacking PS or PS2 stabilization at either the 5′ end or 5′ exit, the whole GalNAc cluster and parts of the sense strand were lost (siRNA-4 in Figures 3 and S2A), almost completely disabling *in vivo* activity of this molecule and highlighting the necessity for stabilization in these positions (Figure 4). Furthermore, unexpected degradation was observed when PS2 was placed at the 5′ exit together with PS2 in the GalNAc branches (siRNA-6 in Figure 3C). This could be due to PS2 distance effects, potentially in combination with increased hydrophobicity and altered protein-binding properties. Further investigation is needed to explain this observation, especially in light of the observed *in vivo* activity of this molecule (Figure 4B).

Surprisingly, a single PS2 at the 5′ end of the sense strand provided long-term stability and good performance *in vivo* (Figures 3 and 4). Notably, the four remaining POs in the GalNAc cluster did not require additional stabilization. Similarly, an additional PS2 at the 5′ end combined with a PS cluster did not further improve stability or activity of the siRNA conjugate. From a synthesis point of view, the PO cluster variant with PS2 at the 5′ end of the sense strand is advantageous, as it avoids the difficult synthesis of PS2-linked trebler and GalNAc and the use of materials with short shelf lives.

Terminal PS2 modifications can stabilize siRNA conjugates and increase RNAi activity

In our approach to specifically substitute stereochemically undefined PS linkages by defined PS2 or PO linkages, we identified

two novel molecular designs with increased RNAi activity: siRNA-12, with PS2 at all tolerated termini and 2 PS at the 5′-antisense terminus, and siRNA-17, which is VP modified at the 5′-antisense terminus and does not contain any undefined PS linkages. Notably, both end stabilization with PS2 and modification with VP independently increase RNAi activity, and an siRNA conjugate with combined PS2 and VP showed an additional increase in performance (Figure 5B). This may be due to a combination of improved stability by PS2 and VP, increased binding affinity to Ago2 by VP, and improved interactions of the siRNA termini with the MID and PAZ domains of Ago2.

PS2 modifications have previously been shown to be well tolerated at specific positions in both strands of an siRNA.[13,14] In addition, siRNAs containing combined PS2 and 2′-OMe modifications have been shown to be more active and associate stronger with Ago2 than unmodified siRNAs, likely due to hydrophobic interactions with the PAZ domain of Ago2.[12,32] While PS orientation in the sense strand does not seem to significantly impact functional properties of the molecule,[3,4] it has been demonstrated that the R_p isomer is preferred at the 5′ end and the S_p isomer is preferred at the 3′ end of the antisense strand.[2–4] Molecular models suggest that this could be driven by differential hydrogen bonding of the R_p- and S_p-configured oxygens with neighboring amino acid side chains in the MID and PAZ domains and by weaker hydrogen bonding of the sulfur in the respective positions.[4] As hydrogen bonds are present for both R_p and S_p isomers at the 5′-antisense terminus, this is in line with the observation that PS2 is less tolerated at this end. It may be that neither the R_p nor S_p diastereomer of the PS linkage is optimally tolerated here and that a PO linkage could be the structurally favored arrangement. In addition to improved binding of VP to the MID domain,[28–30] our molecular design without PS linkages at the VP-modified 5′-antisense terminus is likely to support hydrophilic interactions here. In addition, it has been suggested previously that the preference of R_p isomers at the 5′-antisense terminus may be a consequence of retained 5′-antisense phosphorylation.[2] However, Yang et al. demonstrated that neither PS nor PS2 modification affects 5′-antisense phosphorylation *in vitro*.[13]

For binding of the antisense 3′ end to the PAZ domain, both hydrophilic and hydrophobic models have been proposed.[3,4,32] It may be that hydrophobic interactions of PS2 at the 3′ antisense contribute to increased activity *in vivo*. More likely, PS2 at this position confers increased stability. As R_p isomers are more prone to enzymatic degradation than S_p isomers,[5] it has also been suggested that the preference of S_p at the 3′ antisense is governed by its higher nuclease stability.[2] This raises the question of how the stabilities of PS2, PS R_p isomers, and PS S_p isomers relate to each other. It may be that PS2 confers the greatest nuclease stability, followed by the S_p isomer, and finally the R_p isomer. It should be noted that this study was conducted with antisense strands 19 nt in length and that the exact position of PS2 toward the PAZ domain may vary with siRNA length. Hence, siRNA length may be an additional feature defining the influence of favorable PAZ-domain interactions and siRNA conjugate stability.

Here, we have used PS or VP to stabilize the 5′ end of the antisense strand where PS2 is not tolerated. Likewise, additional ribose modifications beyond 2′-OMe and 2′-F may also result in sufficient metabolic stability to allow for removal of PSs in certain positions. For example, 5′-ribose vinylphosphonate modification[28] or bridged nucleic acids such as locked nucleic acid have been reported to increase the metabolic stability of oligonucleotides,[33,34] although such improvements need to be tested in the context of the siRNA sequence and design. The resulting complexity of this approach is largely determined by the availability of modified building blocks for oligonucleotide synthesis.

PS2-containing siRNA conjugates show high liver and kidney accumulation

We observed slower clearance of PS2-modified siRNA conjugates and thus higher levels in liver and kidney relative to PS-modified molecules 1–6 weeks following administration (Figure 6). Tissue accumulation does not clearly correlate with RNAi activity and is therefore likely not governed by increased binding to Ago2, although previous work indicates improved Ago2 association by PS2.[12,32] Beyond siRNAs, PS2 modifications have also been applied to antisense oligonucleotides (ASOs), short single-stranded oligonucleotides relying on RNA cleavage by RNase H.[35,36] PS2-modified ASOs, specifically ASOs comprising four PS2 linkages, have been reported to show higher levels of liver and kidney accumulation than the respective oligonucleotides with PS,[35] and introducing one, two, and four PS2 modifications into ASOs correlated with increased liver content.[36] In the present work, PS2 modifications did not enhance liver uptake but led to increased siRNA stability *in vitro* and *in vivo*. It remains to be elucidated in future work whether this enhanced siRNA stability contributes to a longer half-life of siRNA in an intracellular depot before entering RNA-induced silencing complex (RISC) or additionally extends the half-life of the formed RISC. The fact that PS2-modified siRNA conjugates showed increased accumulation in kidney and drastically slower clearance rate in this compartment may point toward a different mechanism in the two organs.

While the *in vitro* assays performed in this study to compare knockdown efficacy in primary hepatocytes did not correlate well with the *in vivo* effect of PS2 modifications, they were predictive for the *in vivo* effect of VP. This discrepancy of assessing PS2 effects *in vitro* and *in vivo* has been reported previously, when similar *in vitro* potencies of 3′-antisense Rp and Sp isomers differed significantly *in vivo*.[2] This may suggest that PS2 affects delivery and/or duration of action, neither of which can be assessed in the *in vitro* assays used due to the simplified milieu of 2D cell culture and the necessity for relatively short time series. However, the improvements in tritosome stability comparing PS- and PS2-modified siRNA correlated well with *in vivo* stability as well as with duration of action of *in vivo* knockdown of target transcript.[2]

PS2-modified siRNA conjugates as an option to reduce undefined stereocenters

In this approach, we did not define PS linkages but substituted them by the symmetric linkages PO and PS2 to achieve fully stereodefined

compounds. From a synthesis point of view, PS2 modifications can be easily applied to the internucleotide positions at the siRNA termini. Position-dependent characterization of the stabilization requirements of the GalNAc cluster showed that the cluster does not require additional stabilization when PS2 is present at the 5′ end of the sense strand (Figure 3). Beyond that, we showed that one PS2 can substitute for two PSs at the siRNA termini. In this regard, we reduced the number of PS modifications from ten in the reference design to two in siRNA-12 and none in siRNA-17 (Figures 1A and 5) while introducing three PS2 modifications in both designs. Here, we show that terminal PS2 modifications can positively affect stability and *in vivo* activity of siRNA conjugates, which agrees with previously reported Ago2 molecular modeling, compound stability, and tissue-exposure studies.

Here, we report evidence supporting the use of PS2 internucleotide linkages as a viable alternative to stereodefined amidites for minimizing or eliminating undefined stereocenters, without the need for large-scale synthesis and screening processes. Molecules incorporating PS2 linkages confer the synthetic and analytic advantages of reduced undefined stereocenters while maintaining or, in several cases, enhancing the molecule's stability and *in vivo* activity in a position-dependent manner.

MATERIALS AND METHODS

Building-block synthesis

Syntheses of X4 trebler amidite (**2**) and GalNAc amidite (**5**) were conducted according to earlier published procedures.[18,27] The synthesis routes described for nucleoside thiophosphoramidites[11,12,19,37] are adoptable for the purpose of making thiophosphoramidites of the used trebler and GalNAc. Therefore, the previously described amidite precursors[18] **1** and **4** were successively reacted with first tri(pyrrolidin-1-yl)phosphane in presence of tetrazole and second with N-TMS-imidazole and *S*-(2-mercaptoethyl)benzothioate in a two-step single-pot reaction to form the desired thiophosphoramidites **3** and **6**. Both thiophosphoramidites did not show great chemical stability at ambient conditions. While the trebler thiophosphoramidite (**3**) could be purified by column chromatography with some effort, the GalNAc thiophosphoramidite (**6**) could only be obtained relatively pure by precipitation from heptane (for a detailed description, see supplemental information). Bis-pivaloyloxymethyl (POM)-protected 5′-(E)-VP-2′OMe-uridine phosphoramidite was prepared according to earlier published procedures.[38]

Synthesis of GalNAc-conjugated siRNA

All oligonucleotides were synthesized on an ÄKTA Oligopilot 10 synthesizer using standard phosphoramidite chemistry. Commercially available solid supports and 2′-OMe nucleotide phosphoramidites, 2′-F nucleotide phosphoramidites (all standard protection, ChemGenes, LinkTech), were used according to the manufacturers' recommended procedures. Ancillary reagents were purchased from EMP Biotech and Biosolve. All other reagents and solvents were commercially available and used in standard reagent quality. DMT cleavage was achieved by treatment with 3% dichloroacetic acid in toluene. Coupling was performed using a 0.1 M solution of the phosphoramidite in dry acetonitrile, and BTT was used as activator (0.3 M in acetonitrile). Coupling time was 10 min. Commercially available nucleoside thiophosphoramidites (AM Biotechnologies), trebler thiophosphoramidite (**3**) and GalNAc thiophosphoramidite (**6**), were coupled using a triple couple/wash cycle over a combined period of 60 min. After coupling, a Cap/OX/Cap or Cap/Thio/Cap cycle was applied (Cap: Ac_2O/NMI/lutidine/acetonitrile; oxidizer: 0.1 M I_2 in pyridine/H_2O). PS and PS2 were introduced using 0.05 M ((dimethylamino-methylidene)amino)-3H-1,2,4-dithiazoline-3-thione (DDTT, Chemgenes). Upon completion of the programmed synthesis cycles, a diethylamine (DEA) wash was performed. For 5′-(E)-VP-2′OMe-uridine-modified oligonucleotides the DEA wash was omitted, as it may lead to undesired side-product formation.[39] All oligonucleotides were synthesized in DMT-off mode. The single strands were cleaved off the CPG by 40% aq. methylamine treatment. The resulting crude oligonucleotide was purified by ion-exchange chromatography (SourceQ, 7.5 mL, GE Healthcare) on an ÄKTA Pure HPLC system using a sodium bromide gradient. Product containing fractions were pooled, desalted on a size-exclusion column (Zetadex, EMP Biotech), and lyophilized. All final single-stranded products were analyzed by AEX-HPLC to prove their purity. Identity of the respective single-stranded products was confirmed by LC-MS analysis (for detailed analytical method, data listing, and AEX-HPLC chromatograms, see Tables S1 and S2; Figure S3).

Double-strand formation

To obtain double-strand conjugates, the necessary individual single strands were dissolved in a concentration of 60 OD/mL in H_2O. Both individual oligonucleotide solutions were added to a reaction vessel. For easier reaction monitoring, a titration was performed. The first strand was added in 25% excess over the second strand as determined by UV absorption at 260 nm. The reaction mixture was heated to 80°C for 5 min and then slowly cooled to room temperature. Double-strand formation was monitored by native ion-pairing reverse-phase (IP-RP) HPLC. From the UV area of the residual single strand, the needed amount of the second strand was calculated and added to the reaction mixture. The reaction was heated to 80°C again and slowly cooled to room temperature. This procedure was repeated until less than 5% of residual single strand was detected.

Analytical methods

All final single-stranded products were analyzed by AEX-HPLC to quantify their purity. Purity is stated as the percentage of the UV area under the assigned product signal in the UV trace of the AEX-HPLC analysis of the final product. Identity of the respective single-stranded products (non-modified, PS, PS2, and PS2-GalNAc-conjugated oligonucleotides) was demonstrated by LC-MS analysis. HPLC(-MS) analysis was performed on an Agilent 1260 Infinity II (single quad MS) or on a Waters HClass 1 UPLC-MS instrument. Double-strand purity was analyzed by native IP-RP HPLC and is stated as the percentage of the UV area under the assigned double-stranded product signal. Detailed analytical methods and siRNA conjugate characterization data are listed in Tables S1 and S2.

Stereodefined single-strand analysis by anion exchange chromatography

AEX separations were performed using an LC system Agilent 1200 equipped with a binary solvent delivery pump, a photodiode array detector, and a temperature-controlled column compartment. Data were acquired by OpenLab ChemStation software from Agilent. DNAPac PA200 RS 4.6 × 150 mm, 4 μm particle size (Thermo Fisher, Darmstadt, Germany) was used as chromatographic column applying the following gradient: 40% B hold for 1 min, from 40% to 100% B over 13 min at a flow rate of 0.5 mL/min at 30°C. Mobile phase A consisted of 20 mM Tris (pH 9.0 with NaOH 1 M) in H_2O (v/v), and mobile phase B consisted of 20 mM Tris (pH 9 with NaOH 1 M), 1.25 M NaCl in H_2O (v/v) (method e, Table S1).

Quantification of oligonucleotides

Oligonucleotides were quantified by their UV absorption at 260 nm in water using a NanoDrop Photometer (VWR, Darmstadt, Germany). A conversion factor of 30 OD = 1 mg (33 μg = 1 OD) for single-stranded RNA and 25 OD = 1 mg (40 μg = 1 OD) for double-stranded siRNA conjugates was used. Calculation and comparison of extinction coefficients by nearest-neighbor method confirmed the accuracy of this method. Hyperchromicity experienced upon hybridization also confirmed accuracy of the conversion factor for double-stranded siRNA conjugates (data not shown). Concentration in mg/mL and doses in mg/kg refer to the RNA part of the conjugate only, ensuring equal molarity used in *in vitro* and *in vivo* experiments across all researched conjugates.

Melting curve analysis

Melting curve experiments were performed on a Cary3500 (Agilent) UV-vis spectrometer. Temperature ramp was set to 1 K per minute, and the concentration was chosen to be at 0.5 absorption in the spectrometer in PBS buffer (Dulbecco's PBS, MS01AM1007, BioWest). siRNA conjugates were placed in a quartz cuvette (Hellma HL114-10-40) with PBS buffer, and the thermal heating/cooling cycle was applied three times. Any stated T_m values are the mean of three repeated measurements.

In vitro siRNA treatment and RNA isolation

Cells were treated as previously described with minor changes.[27] In brief, plateable, male murine primary hepatocytes (MSCP10, various lots; Thermo Fisher Scientific, Waltham, MA, USA) were thawed and reconstituted in Williams E medium (A1217601; Thermo Fisher Scientific) supplemented with primary hepatocyte thawing and plating supplements (CM3000; Thermo Fisher Scientific). 25,000 mouse primary hepatocytes were plated into collagen I pre-coated 96-well plates (Ref.: A11428-28-03; Life Technologies, Carlsbad, CA, USA). siRNA was pre-diluted in the same medium (5× concentrated) for each concentration and added to the cells at a final volume of 125 μL per well. An equivalent volume of water was used as an untreated control. Thereafter, cells were cultured at 37°C and 5% CO_2. The supernatant was discarded 24 h after treatment, cells were washed in cold PBS, and 250 μL of RNA-Lysis Buffer S was added. Following a 15-min incubation at room temperature, plates were stored at −80°C until RNA isolation was performed according to the manufacturer's protocol (InviTrap RNA Cell HTS 96 Kit, #7061300400, Stratec, Birkenfeld, Germany).

TaqMan analysis

For MultiPlex TaqMan analysis of AT3 and ActB or for AT3 and ApoB, 10 μL of isolated RNA for each treatment group was mixed with 10 μL of PCR master mix (UF-LP5X-RT0101; Eurogentec, Seraing, Belgium) containing 400 nM AT3 primers and 300 nM ActB primers or 300 nM AT3 primers and 300 nM ApoB primers, as well as 100 nM of each probe, and 0.5 U M-MLV reverse transcriptase (cat. #M368C; Promega, Madison, WI, USA). TaqMan analysis was performed in a 384-well plate with a 10-min RT step at 48°C, 3 min initial denaturation at 95°C, and 40 cycles of 95°C for 3 s and 60°C for 20 s in a QuantStudio 6 (Applied Biosystems, Waltham, MA, USA) RT-cycler. TaqMan primer and probes were purchased from BioTEZ (Berlin, Germany) or Eurogentec (Seraing, Belgium). The following amplicon sets were used. AT3 upper: 5′-CAT GGG CCT CAT TGA TCT CTT C-3′; AT3 lower: 5′-GGT CGT CCC TGC CTC CA-3′; AT3 probe: 5′-FAM-AGC CCT GAA AAG TCC CAA CTC CCA GG-BHQ1-3′. ActB upper: 5′-CCT AAG GCC AAC CGT GAA AAG-3′; ActB lower: 5′-AGG CAT ACA GGG ACA GCA CAG-3′; ActB probe: 5′-YY-TGA GAC CTT CAA CAC CCC AGC CAT GTA C-BHQ1-3′. ApoB upper: 5′-AAA GAG GCC AGT CAA GCT GTT C-3′; ApoB lower: 5′-GGT GGG ATC ACT TCT GTT TTG G-3′; ApoB probe: 5′-YY-CAG CAA CAC ACT GCA TCT GGT CTC TAC CA-BHQ1-3′. (FAM, 6-carboxyfluorescein; YY, Yakima yellow; BHQ1, Black Hole Quencher 1).

Stability assays of GalNAc-siRNA conjugates

For *in vitro* stability analysis, siRNA conjugates were incubated in serum or acidified tritosome lysates as described previously.[27] For serum stability assessment, 15 μL of FBS (cat. #P30-3306; PAN Biotech, Aidenbach, Germany) was mixed with 5 μL of siRNA (20 μM) and incubated for 24 h. siRNA conjugates were incubated for 0, 24, or 96 h in Sprague-Dawley rat liver tritosomes (R0610.LT; Sekisui Xenotech, Kansas City, MO, USA). To mimic the acidified environment, tritosomes were mixed 10:1 with low pH buffer (1.5 M acetic acid, 1.5 M sodium acetate, pH 4.75). 30 μL of these acidified tritosomes was mixed with 10 μL of siRNA (20 μM) and incubated for the indicated times at 37°C. For incubation times longer than 24 h, fresh tritosomes were added every 24 h. Following incubation, RNA was isolated with the Clarity OTX Starter Kit-Cartridges (KSO-8494; Phenomenex, Germany) according to the manufacturer's protocol for biological fluids. Lyophilized RNA was reconstituted in 30 μL of H_2O, 12 μL of reconstituted RNA was mixed with 4 μL of loading buffer (Novex TBE-Sample Buffer high density [5×], cat. #LC6678; Thermo Fisher Scientific), and 5 μL was loaded into 20% Tris-borate-EDTA (TBE)-PAGE for separation and qualitative semi-quantitative analysis. PAGE was run at 120 V for 2 h, and RNA was visualized with ethidium bromide solution (cat. #15585011; Thermo Fisher Scientific) staining, with digital images acquired with a Bio-Rad Gel Doc EZ Imager. LC-tandem MS analysis of

the resulting metabolites was performed under denaturing conditions (Table S1 and Figure S2).

In vivo experiments

In vivo experiments with C57BL/6 mice were performed at Experimental Pharmacology & Oncology Berlin-Buch (EPO, Berlin, Germany) in accordance with the United Kingdom Co-ordinating Committee on Cancer Research regulations for the Welfare of Animals and of the German Animal Protection Law and approved by the local responsible authorities. Compounds were injected subcutaneously at the indicated concentration into the scapular region of mice. The administration volume was adjusted according to the body weight (10 mL/kg). Blood was collected by orbital sinus bleeding, and serum was extracted by centrifugation using Microvette 500 Z-Gel (Sarstedt, Nümbrecht, Germany) and transferred into Eppendorf tubes for storage at −20°C. Serum AT3 levels in mice were analyzed with a mouse ELISA kit (ab108800; Abcam, Cambridge, UK) according to the manufacturer's protocol. Typically, serum was diluted 1:8,000 up to 1:10,000 in the recommended diluent.

Stem-loop qPCR quantification of siRNA

For siRNA quantification, frozen tissue samples were weighed, and per 1 mg tissue 7.5 µL lysis buffer (QuantiGene Sample Processing Kit, tissues, cat. #QS0106; Thermo Fisher Scientific) was added accordingly. Next, a tungsten carbide bead (ref. 69997; Qiagen, Venlo, Netherlands) was added, and tissue lysed by applying 5 × 30-s 27.5-Hz cycles in a TissueLyser (Retch Type MM300; Qiagen). Thereafter, lysates were incubated for 30 min at 65°C, then for 10 min at room temperature, and centrifuged at 21,000 × *g*. Each 50 µL of the supernatant was aliquoted in 96-well plates and stored at −80°C or subjected to further analysis. For quantitation of the antisense strand in tissue lysates, three independent standard rows were generated by serial dilution of respective siRNAs in the matrix of interest obtained from the vehicle group. To assess precision of the assay and determine the detection range, an independent serial dilution of the same siRNA in respective matrix was generated as quality control (QC). Upper and lower limits of detection were defined by less than 30% deviation of QC from standard curve values. Unknown antisense concentrations in tissue lysates were interpolated by nonlinear 5-parameter-fit with GraphPad Prism 10 (Dotmatics, Boston, MA, USA) based on the standard curve generated. Stem-loop primers were designed as described earlier.[40,41] Standard, QC, and samples of unknown siRNA concentration were processed in parallel in a two-step RT-qPCR. For the RT reaction, lysate was diluted 400-fold in H_2O and 4 µL thereof was incubated in a 384-well cycler for 10 min at 95°C. Next, 6 µL master mix containing 0.5 pmol stem-loop primer 5′-GTC GTA TCC AGT GCA GGG TCC GAG GTA TTC GCA CTG GAT ACG ACT TAA CA-3′ was added and incubated for 30 min at 16°C, 30 min at 42°C, 5 min at 85°C, and finally at 4°C. Next, 5 µL of the RT samples was diluted in 20 µL H_2O, and 5 µL of this diluted RT sample was added to 15 µL of qPCR reaction mix containing 9 pmol 5′-GTG CAG GGT CCG AGG T-3′, 9 pmol 5′-CGT TGA AGT AAA TGG TG-3′, and 4 pmol 5′-FAM-TCG CAC TGG ATA CG-MGB-3′. The PCR was conducted in a QuantStudio 6 real-time cycler (Thermo Fisher Scientific) with the following program: 3 min at 95°C followed by 40 cycles of 3 s at 95°C and 20 s at 60°C.

Statistical analysis

One-way ANOVA were performed using the Kruskal-Wallis test with Dunn's multiple comparisons (GraphPad Prism 10.1.2 [324]; Dotmatics).

DATA AND CODE AVAILABILITY

The authors confirm that the data supporting the findings of this study are available within the article and/or its supplemental information.

ACKNOWLEDGMENTS

The authors thank Lisa Bethke and Vivien Hehne for excellent support in bioassay development and analyses, and Mona Bill for development of the analytical method for stereo-defined AEX. All work in this study is sponsored by Silence Therapeutics with no additional funding or grants.

AUTHOR CONTRIBUTIONS

L.B., J.H., A.W., E.M., and M.W.L. conceptualized the studies. S.S., S.R., M.G., A.W., J.H., and N.W. designed experiments, analyzed the results, and prepared figures. M.G. developed chemistry analytics protocols. All authors contributed to writing of the manuscript.

DECLARATION OF INTERESTS

All authors are employees of and have stock options in Silence Therapeutics GmbH. A patent has been granted for the initial findings from this work: US Patent for "Nucleic acids for inhibiting expression of a target gene comprising phosphorodithioate linkages" (Patent #11873489).

SUPPLEMENTAL INFORMATION

Supplemental information can be found online at https://doi.org/10.1016/j.omtn.2024.102336.

REFERENCES

1. Burgers, P.M., and Eckstein, F. (1978). Synthesis of dinucleoside monophosphorothioates via addition of sulphur to phosphite triesters. Tetrahedron Lett. *19*, 3835–3838. https://doi.org/10.1016/s0040-4039(01)95072-5.

2. Sakamuri, S., Eltepu, L., Liu, D., Lam, S., Meade, B.R., Liu, B., Dello Iacono, G., Kabakibi, A., Luukkonen, L., Leedom, T., et al. (2020). Impact of Phosphorothioate Chirality on Double-Stranded siRNAs: A Systematic Evaluation of Stereopure siRNA Designs. Chembiochem *21*, 1304–1308. https://doi.org/10.1002/cbic.201900630.

3. Liu, W., Iwamoto, N., Marappan, S., Luu, K., Tripathi, S., Purcell-Estabrook, E., Shelke, J.D., Shah, H., Lamattina, A., Pan, Q., et al. (2023). Impact of stereopure chimeric backbone chemistries on the potency and durability of gene silencing by RNA interference. Nucleic Acids Res. *51*, 4126–4147. https://doi.org/10.1093/nar/gkad268.

4. Jahns, H., Taneja, N., Willoughby, J.L.S., Akabane-Nakata, M., Brown, C.R., Nguyen, T., Bisbe, A., Matsuda, S., Hettinger, M., Manoharan, R.M., et al. (2022). Chirality matters: stereo-defined phosphorothioate linkages at the termini of small interfering RNAs improve pharmacology in vivo. Nucleic Acids Res. *50*, 1221–1240. https://doi.org/10.1093/nar/gkab544.

5. Iwamoto, N., Butler, D.C.D., Svrzikapa, N., Mohapatra, S., Zlatev, I., Sah, D.W.Y., Apponi, L.H., Standley, S.M., Standley, S.M., Lu, G., et al. (2017). Control of phosphorothioate stereochemistry substantially increases the efficacy of antisense oligonucleotides. Nat. Biotechnol. *35*, 845–851. https://doi.org/10.1038/nbt.3948.

6. Arrico, L., Stolfi, C., Marafini, I., Monteleone, G., Demartis, S., Bellinvia, S., Viti, F., McNulty, M., Cabani, I., Falezza, A., and Di Bari, L. (2022). Inhomogeneous Diastereomeric Composition of Mongersen Antisense Phosphorothioate

Oligonucleotide Preparations and Related Pharmacological Activity Impairment. Nucleic Acid Ther. *32*, 312–320. https://doi.org/10.1089/nat.2021.0089.

7. Egli, M., and Manoharan, M. (2023). Chemistry, structure and function of approved oligonucleotide therapeutics. Nucleic Acids Res. *51*, 2529–2573. https://doi.org/10.1093/nar/gkad067.

8. Sakamuri, S., Liu, D., Eltepu, L., Liu, B., Reboton, L.J., Preston, R., and Bradshaw, C.W. (2020). Identification of a Tricyclic PIII Chiral Auxiliary for Solid-Supported Synthesis of Stereopure Phosphorothioate-Containing Oligonucleotides. Chembiochem *21*, 1298–1303. https://doi.org/10.1002/cbic.201900631.

9. Knouse, K.W., deGruyter, J.N., Schmidt, M.A., Zheng, B., Vantourout, J.C., Kingston, C., Mercer, S.E., Mcdonald, I.M., Olson, R.E., Zhu, Y., et al. (2018). Unlocking P(V): Reagents for chiral phosphorothioate synthesis. Science *361*, 1234–1238. https://doi.org/10.1126/science.aau3369.

10. Rosenqvist, P., Saari, V., Pajuniemi, E., Gimenez Molina, A., Ora, M., Horvath, A., and Virta, P. (2023). Stereo-Controlled Liquid Phase Synthesis of Phosphorothioate Oligonucleotides on a Soluble Support. J. Org. Chem. *88*, 10156–10163. https://doi.org/10.1021/acs.joc.3c01006.

11. Brill, W.K.D., Tang, J.Y., Ma, Y.X., and Caruthers, M.H. (1989). Synthesis of oligodeoxynucleoside phosphorodithioates via thioamidites. J. Am. Chem. Soc. *111*, 2321–2322. https://doi.org/10.1021/ja00188a066.

12. Wu, S.Y., Yang, X., Gharpure, K.M., Hatakeyama, H., Egli, M., McGuire, M.H., Nagaraja, A.S., Miyake, T.M., Rupaimoole, R., Pecot, C.V., et al. (2014). 2′-OMe-phosphorodithioate-modified siRNAs show increased loading into the RISC complex and enhanced anti-tumour activity. Nat. Commun. *5*, 3459. https://doi.org/10.1038/ncomms4459.

13. Yang, X., Sierant, M., Janicka, M., Peczek, L., Martinez, C., Hassell, T., Li, N., Li, X., Wang, T., and Nawrot, B. (2012). Gene Silencing Activity of siRNA Molecules Containing Phosphorodithioate Substitutions. ACS Chem. Biol. *7*, 1214–1220. https://doi.org/10.1021/cb300078e.

14. Rodriguez-Aguayo, C., Bayraktar, E., Ivan, C., Aslan, B., Mai, J., He, G., Mangala, L.S., Jiang, D., Nagaraja, A.S., Ozpolat, B., et al. (2019). PTGER3 induces ovary tumorigenesis and confers resistance to cisplatin therapy through up-regulation Ras-MAPK/Erk-ETS1-ELK1/CFTR1 axis. EBioMedicine *40*, 290–304. https://doi.org/10.1016/j.ebiom.2018.11.045.

15. Grandas, A., Marshall, W.S., Nielsen, J., and Caruthers, M.H. (1989). Synthesis of deoxycytidine oligomers containing phosphorodithioate linkages. Tetrahedron Lett. *30*, 543–546. https://doi.org/10.1016/s0040-4039(00)95248-1.

16. Sehgal, A., Barros, S., Ivanciu, L., Cooley, B., Qin, J., Racie, T., Hettinger, J., Carioto, M., Jiang, Y., Brodsky, J., et al. (2015). An RNAi therapeutic targeting antithrombin to rebalance the coagulation system and promote hemostasis in hemophilia. Nat. Med. *21*, 492–497. https://doi.org/10.1038/nm.3847.

17. Kumar, V., and Turnbull, W.B. (2023). Targeted delivery of oligonucleotides using multivalent protein–carbohydrate interactions. Chem. Soc. Rev. *52*, 1273–1287. https://doi.org/10.1039/d2cs00788f.

18. Frauendorf, C., and Cameron, M. (2017). Nucleic Acid Linked to a Trivalent Glycoconjugate. US patent US11912993 B2. filed May 5, 2017, and granted February 27, 2024.

19. Wiesler, W.T., and Caruthers, M.H. (1996). Synthesis of Phosphorodithioate DNA via Sulfur-Linked, Base-Labile Protecting Groups1. J. Org. Chem. *61*, 4272–4281. https://doi.org/10.1021/jo960274y.

20. Yang, X. (2016). Solid-Phase Synthesis of Oligodeoxynucleotide Analogs Containing Phosphorodithioate Linkages. Curr. Protoc. Nucleic Acid Chem. *66*, 4.71.1–4.71.14. https://doi.org/10.1002/cpnc.13.

21. Thayer, J.R., Wu, Y., Hansen, E., Angelino, M.D., and Rao, S. (2011). Separation of oligonucleotide phosphorothioate diastereoisomers by pellicular anion-exchange chromatography. J. Chromatogr. A *1218*, 802–808. https://doi.org/10.1016/j.chroma.2010.12.051.

22. Piao, X., Wang, H., Binzel, D.W., and Guo, P. (2018). Assessment and comparison of thermal stability of phosphorothioate-DNA, DNA, RNA, 2′-F RNA, and LNA in the context of Phi29 pRNA 3WJ. RNA *24*, 67–76. https://doi.org/10.1261/rna.063057.117.

23. Cummins, L., Graff, D., Beaton, G., Marshall, W.S., and Caruthers, M.H. (1996). Biochemical and Physicochemical Properties of Phosphorodithioate DNA. Biochemistry *35*, 8734–8741. https://doi.org/10.1021/bi960318x.

24. McDougall, R., Ramsden, D., Agarwal, S., Agarwal, S., Aluri, K., Arciprete, M., Brown, C., Castellanos-Rizaldos, E., Charisse, K., Chong, S., et al. (2022). The Nonclinical Disposition and Pharmacokinetic/Pharmacodynamic Properties of N -Acetylgalactosamine–Conjugated Small Interfering RNA Are Highly Predictable and Build Confidence in Translation to Human. Drug Metab. Dispos. *50*, 781–797. https://doi.org/10.1124/dmd.121.000428.

25. Dautry-Varsat, A., Ciechanover, A., and Lodish, H.F. (1983). pH and the recycling of transferrin during receptor-mediated endocytosis. Proc. Natl. Acad. Sci. USA *80*, 2258–2262. https://doi.org/10.1073/pnas.80.8.2258.

26. Kandasamy, P., Mori, S., Matsuda, S., Erande, N., Datta, D., Willoughby, J.L.S., Taneja, N., O'Shea, J., Bisbe, A., Manoharan, R.M., et al. (2023). Metabolically Stable Anomeric Linkages Containing GalNAc–siRNA Conjugates: An Interplay among ASGPR, Glycosidase, and RISC Pathways. J. Med. Chem. *66*, 2506–2523. https://doi.org/10.1021/acs.jmedchem.2c01337.

27. Weingärtner, A., Bethge, L., Weiss, L., Sternberger, M., and Lindholm, M.W. (2020). Less Is More: Novel Hepatocyte-Targeted siRNA Conjugates for Treatment of Liver-Related Disorders. Mol. Ther. Nucleic Acids *21*, 242–250. https://doi.org/10.1016/j.omtn.2020.05.026.

28. Haraszti, R.A., Roux, L., Coles, A.H., Turanov, A.A., Alterman, J.F., Echeverria, D., Godinho, B.M.D.C., Aronin, N., and Khvorova, A. (2017). 5′-Vinylphosphonate improves tissue accumulation and efficacy of conjugated siRNAs in vivo. Nucleic Acids Res. *45*, 7581–7592. https://doi.org/10.1093/nar/gkx507.

29. Parmar, R., Willoughby, J.L.S., Liu, J., Foster, D.J., Brigham, B., Theile, C.S., Charisse, K., Akinc, A., Guidry, E., Pei, Y., et al. (2016). 5′-(E)-Vinylphosphonate: A Stable Phosphate Mimic Can Improve the RNAi Activity of siRNA–GalNAc Conjugates. Chembiochem *17*, 985–989. https://doi.org/10.1002/cbic.201600130.

30. Elkayam, E., Parmar, R., Brown, C.R., Willoughby, J.L., Theile, C.S., Manoharan, M., and Joshua-Tor, L. (2017). siRNA carrying an (E)-vinylphosphonate moiety at the 5′ end of the guide strand augments gene silencing by enhanced binding to human Argonaute-2. Nucleic Acids Res. *45*, 3528–3536. https://doi.org/10.1093/nar/gkw1171.

31. Weingärtner, A., and Bethge, L. (2019). siRNAs with vinylphosphonate at the 5′ end of the antisense strand. US patent US11560563B2. filed April 5, 2019, and granted January 24, 2023.

32. Pallan, P.S., Yang, X., Sierant, M., Abeydeera, N.D., Hassell, T., Martinez, C., Janicka, M., Nawrot, B., and Egli, M. (2014). Crystal structure, stability and Ago2 affinity of phosphorodithioate-modified RNAs. RSC Adv. *4*, 64901–64904. https://doi.org/10.1039/c4ra10986d.

33. Obika, S., Nanbu, D., Hari, Y., Morio, K.i., In, Y., Ishida, T., and Imanishi, T. (1997). Synthesis of 2′-O,4′-C-methyleneuridine and -cytidine. Novel bicyclic nucleosides having a fixed C3, -endo sugar puckering. Tetrahedron Lett. *38*, 8735–8738. https://doi.org/10.1016/s0040-4039(97)10322-7.

34. Elmén, J., Thonberg, H., Ljungberg, K., Frieden, M., Westergaard, M., Xu, Y., Wahren, B., Liang, Z., Ørum, H., Koch, T., and Wahlestedt, C. (2005). Locked nucleic acid (LNA) mediated improvements in siRNA stability and functionality. Nucleic Acids Res. *33*, 439–447. https://doi.org/10.1093/nar/gki193.

35. Duschmalé, J., Schäublin, A., Funder, E., Schmidt, S., Kiełpiński, Ł.J., Nymark, H., Jensen, K., Koch, T., Duschmalé, M., Koller, E., et al. (2022). Investigating discovery strategies and pharmacological properties of stereodefined phosphorodithioate LNA gapmers. Mol. Ther. Nucleic Acids *29*, 176–188. https://doi.org/10.1016/j.omtn.2022.06.010.

36. Bleicher, K., Hansen, H.F., Koch, T., Worm, J., Schaeublin, A., Funder, E., Duschmalé, J., Joenson, L., Li, M., Duschmalé, M.B., Wu, Y., and Shu, X. (2020). Oligonucleotides Comprising a Phosphorodithioate Internucleoside Linkage. US patent EP3728592 B1. filed December 21, 2018, and granted May 29, 2024.

37. Brill, W.K.-D., Nielsen, J., and Caruthers, M.H. (1988). Synthesis of dinucleoside phosphorodithioates via thioamidites. Tetrahedron Lett. *29*, 5517–5520. https://doi.org/10.1016/s0040-4039(00)80801-1.

38. Parmar, R.G., Brown, C.R., Matsuda, S., Willoughby, J.L.S., Theile, C.S., Charissé, K., Foster, D.J., Zlatev, I., Jadhav, V., Maier, M.A., et al. (2018). Facile Synthesis, Geometry, and 2′-Substituent-Dependent in Vivo Activity of 5′-(E)- and

5′-(Z)-Vinylphosphonate-Modified siRNA Conjugates. J. Med. Chem. *61*, 734–744. https://doi.org/10.1021/acs.jmedchem.7b01147.

39. O'Shea, J., Theile, C.S., Das, R., Babu, I.R., Charisse, K., Manoharan, M., Maier, M.A., and Zlatev, I. (2018). An efficient deprotection method for 5′-[O,O-bis(pivaloyloxymethyl)]-(E)-vinylphosphonate containing oligonucleotides. Tetrahedron *74*, 6182–6186. https://doi.org/10.1016/j.tet.2018.09.008.

40. Chen, C., Ridzon, D.A., Broomer, A.J., Zhou, Z., Lee, D.H., Nguyen, J.T., Barbisin, M., Xu, N.L., Mahuvakar, V.R., Andersen, M.R., et al. (2005). Real-time quantification of microRNAs by stem–loop RT–PCR. Nucleic Acids Res. *33*, e179. https://doi.org/10.1093/nar/gni178.

41. Jung, U., Jiang, X., Kaufmann, S.H.E., and Patzel, V. (2013). A universal TaqMan-based RT-PCR protocol for cost-efficient detection of small noncoding RNA. RNA *19*, 1864–1873. https://doi.org/10.1261/rna.040501.113.